Food Chemistry: X 21 (2024) 101230

Contents lists available at ScienceDirect

Food Chemistry: X

journal homepage: www.sciencedirect.com/journal/food-chemistry-x

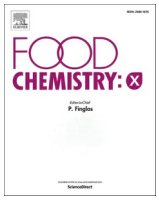

Self-assembled nanoparticles of acid-induced fish (*Cyprinus carpio* L.) scale gelatin: Structure, physicochemical properties, and application for loading curcumin

Haoxin Li [a,b], Wan Aida Wan Mustapha [b], Jia Liu [a,c,d,*], Xiaoping Zhang [e]

[a] The Key Laboratory of Environmental Pollution Monitoring and Disease Control, Ministry of Education, Guizhou Provincial Engineering Research Center of Ecological Food Innovation, School of Public Health, Guizhou Medical University, Guiyang 550025, China
[b] Department of Food Sciences, Faculty of Science and Technology, Universiti Kebangsaan Malaysia (UKM), Bangi 43600, Malaysia
[c] School of Liquor & Food Engineering, Guizhou University, Guiyang 550025, China
[d] Institute of Food Processing Technology, Guizhou Academy of Agricultural Sciences, Guiyang 550006, China
[e] Guizhou Fishery Research Institute, Guizhou Academy of Agricultural Science, Guiyang 550025, China

ARTICLE INFO

Keywords:
Acid hydrolysis
Fish scale gelatin
Curcumin
Self-assembly
Sustained release

ABSTRACT

This work expands the functionality of fish scale gelatin (FSG) as a carrier of hydrophobic bioactive substances. The hydrophobicity of FSG was enhanced to promote its interaction with hydrophobic curcumin and to increase its bioavailability. This results in a remarkable increase in the curcumin loading capacity of acid-hydrolyzed FSG (HFSG) from 1.08 ± 0.08 μg/mg (0 h) to 9.15 ± 0.21 μg/mg (3 h). The amino acid composition indicated that acid hydrolysis effectively increased the ratio of hydrophobic amino acids of FSG. Acid hydrolysis facilitated the transformation of the α-helical conformation into a β-sheet structure. Hydrophobic interactions between HFSG and curcumin were strengthened by moderate acid hydrolysis. A sustained-release profile emerged for the curcumin-loaded HFSG during simulated gastrointestinal digestion, thereby improving the bioaccessibility and bioavailability of curcumin. These findings contribute to the application of acid hydrolysis in modifying FSG for enhanced hydrophobicity and curcumin loading capacity in the food industry.

1. Introduction

Gelatin is widely used in the food, pharmaceutical, and cosmetic industries due to its unique multi-functional properties (e.g. gelling properties, foaming properties, emulsifying properties, film-forming properties). With the rapid development of food, pharmaceutical and other industries, the demand for gelatin has soared. It is reported that 98.5 % of global commercial gelatin is derived from mammalian pig skin (46 %), cowhide (29.4 %), pig bone, and cow bone (23.1 %) (Karim & Bhat, 2009). However, the widespread adoption of mammalian gelatin faces considerable limitations nowadays owing to pressing concerns related to food safety – particularly its prion pathogen transmission potential. Moreover, the application of mammalian gelatin has been restricted by considerations rooted in religious sentiments. In response to the growing demand for mammalian gelatin, researchers are actively investigating a range of alternatives, including fish gelatin (Huang et al., 2018; Huang et al., 2017; Li et al., 2021), poultry gelatin (Aidat, Belkacemi, Belalia, Zainol, & Barhoum, 2023), insect gelatin (Chua, Lim, Thoo, Neo, & Tan, 2023), and polysaccharide-protein complexes (Li, Tang, Lei, Wang, & Liu, 2021; Sha et al., 2014), etc. Among them, fish gelatin is widely used as a potential alternative owing to physicochemical properties similar to those of mammalian gelatin. However, compared with mammalian gelatin, the main technical bottlenecks for fish gelatin include variable quality, inferior rheological behaviors and gel properties, limiting its large-scale application (Huang et al., 2019). To address these shortcomings, various techniques have been developed to enhance the functional properties of fish gelatin. These include modifying the gelatin extraction parameters (Kołodziejska, Skierka, Sadowska, Kołodziejski, & Niecikowska, 2008; Li et al., 2021), enzymatically modifying fish gelatin (Jongjareonrak, Benjakul, Visessanguan, & Tanaka, 2006), phosphorylating fish gelatin (Huang et al., 2018; Kaewruang, Benjakul, & Prodpran, 2014), the addition of protein or polysaccharide (Li et al., 2021), chemical crosslinking (Mohtar, Perera, & Hemar, 2014), and physical treatments (Bhat & Karim, 2009).

* Corresponding author.
E-mail address: mcgrady456@163.com (J. Liu).

https://doi.org/10.1016/j.fochx.2024.101230
Received 5 August 2023; Received in revised form 13 February 2024; Accepted 14 February 2024
Available online 18 February 2024

Given the constraints associated with the aforementioned methods, however, it is important to acknowledge detrimental factors such as the high cost of enzymes, concerns about food safety stemming from chemical crosslinking agents (which might induce genotoxic effects in food systems) or organic solvents (which pose potential harm to human health), and heightened instability resulting from the formation of complex coacervates and physical treatments. Acid hydrolysis has been verified as an effective and cost-saving method for enhancing the functional properties of food proteins and preparing nanoparticles. In light of the fact that acid-induced protein hydrolysate is used as a delivery system for encapsulating hydrophobic molecules, no organic solvents or chemical denaturants are required. When a protein molecule is exposed to a polar pH environment, the protein molecule is prone to folding or partially folding. When the molecule shifts to a neutral pH, the electrostatic repulsion within the molecule greatly weakens and a certain degree of refolding occurs. Thus, a flexible, self-assembled protein conformation is generated and effectively enhances its carrier properties, with increased surface hydrophobicity, amphiphilic balance, and advanced functional properties (Pan, Luo, Gan, Baek, & Zhong, 2014).

Studies have shown that structural changes in soy isolate protein resulted in significant functional improvements such as surface hydrophobicity and emulsification activity by pH-shifting treatment (Jiang, Chen, & Xiong, 2009). It has been reported that citric acid-mediated cross-linking not only improved the surface hydrophobicity of whey protein under non-acidic aqueous conditions but also enhanced its emulsification and foaming capacity (Li et al., 2018). Pan & Zhong (2016) constructed zein-casein nanoparticles with a particle size of less than 100 nm by a pH-driven method and maintained a stable dispersion state during 30 days of storage. Curcumin was encapsulated in zein-caseinate nanoparticles by the pH-driven method, and the encapsulation efficiency reached 87.1 % (Wang, Xue, & Zhang, 2019). Additionally, whey protein hydrolysate nanoparticles encapsulated by gallic acid were prepared by the reverse-solvent method, and the cross-linking of citric acid resulted in smaller particles with higher encapsulation efficiency (Nourbakhsh et al., 2017). Remarkably, there remains a paucity of information concerning the utilization of self-assembled nanoparticles derived from fish gelatin. For example, nanoparticles that self-assembled through the hydrolysis of pepsin or the phosphorylation of fish gelatin exhibited noteworthy improvements in both gel strength and emulsion stability (Cen et al., 2022; Wu et al., 2022). Chen et al. (2023) employed microbial transglutaminase (MTG) to form self-assemblies from grass carp scale gelatin, leading to an augmented release of bioactive peptides during simulated gastrointestinal digestion. However, to the best of our knowledge, attempting to construct self-assembled nanoparticle carriers from acid-hydrolyzed fish scale gelatin (HFSG) has not been reported. Moreover, the mechanism pertaining to the influence of the duration of the acid hydrolysis on the structural properties of HFSG and its subsequent impact on curcumin loading capacity remains unclear.

Hence, it was hypothesized that the acid-induced hydrolysis of FSG could enhance its functionality in loading hydrophobic bioactive substances. To test this hypothesis, the effects of varying the acid hydrolysis durations (1 h, 2 h, 3 h, 4 h, 6 h, and 8 h) on the molecular structural properties of FSG and their curcumin loading capacity (hydrophobic molecules' model) were investigated. In addition, fluorescence spectroscopy and confocal laser scanning microscopy (CLSM) were employed to elucidate the underlying mechanism of the interaction between curcumin and FSG, with or without acid hydrolysis. Furthermore, the stability and release properties of curcumin from CL-FSG and CL-HFSG during *in vitro* gastrointestinal digestion were assessed. In summary, this study offers insights into promoting the use of HFSG in forming self-assemblies and its potential as a carrier for hydrophobic bioactive substances.

2. Material and methods

2.1. Materials

Fish (*Cyprinus carpio* L.) scales (FS) were harvested at the Guizhou Fisheries Research Institute experimental base (Guiyang City, Guizhou Province, China). The FS were washed with tap water and placed in an oven (WGL-65B, Taisite Instrument Co. Ltd., Tianjin, China) at 40 °C for 24 h to eliminate residual water. The dried FS were stored in a desiccator before use. Curcumin (purity > 90 %) was purchased from Merck-Schuchardt Co. (Hohenbrunn, Germany). Pre-stained protein markers (bands 1–8: 55, 65, 90, 130, 165, 210, 270 and 320 kDa) were purchased from Wolsen Biotechnology Co., Ltd (Shanghai, China). Sodium dodecyl sulfate (SDS) and Coomassie Brilliant Blue R-250 were purchased from Merck (Darmstadt, Germany). Sodium azide and acetonitrile (chromatographic grade) were procured from Chron Chemicals Co., Ltd. (Cheng Du, China). Pepsin (4000 U/g) and pancreatin (3000 U/g) were supplied by Solarbio Science & Technology Co., Ltd. (Beijing, China) and Yuanye Science & Technology Co., Ltd. (Shanghai, China), respectively. Other analytical grade chemicals were obtained from Solarbio Science & Technology Co., Ltd. (Beijing, China).

2.2. Preparation of acid-hydrolyzed FSG (HFSG)

The extraction of FSG was carried out according to our preliminary experiments (Li et al., 2021). The HFSG was prepared by adding defined amounts of citric acid (0.2 M) for 0, 1, 2, 3, 4, 6, and 8 h, and neutralized to pH 7.0 with 0.1 mol/L NaOH at the end of the respective reaction. The resulting solution was dialyzed (molecular weight cutoff = 14,000 Da) overnight to remove excess acid ions. Subsequently, the dialyzed sample was freeze-dried, and the resulting powdered sample was stored at 4 ℃ for further analysis. At least three replicates were performed for each experiment.

2.3. Preparation of CL-FSG and CL-HFSG

The freeze-dried FSG and HFSG (40 mg) samples were initially dissolved in 20 mL of distilled water, following the method described by Liu et al. (2013). The curcumin powder (10 mg) was then dissolved in a 20 mL sample solution. The solution was subsequently homogenized at 12,000 rpm for 5 min via a homogenizer (IKA T18 basic, IKA-Werke GmbH & Co., Staufen, Germany). The homogenized suspension was continuously stirred in a 30 ± 1 °C water bath with 300 rpm agitation for 24 h. The curcumin concentration of the CL-FSG or CL-HFSG solution was analyzed by HPLC based on the method of Liu et al. (2013). Specifically, curcumin was extracted from the hydrophobic region by combining CL-FSG or CL-HFSG solution with methanol (in a ratio of 1:4, *v/v*). After vortexing for 2 min, the mixtures were centrifuged (L535R-1, Xiangyi Centrifuge Instrument, Hunan, China) (5600 g, 10 min, 25 °C) and filtered through a 0.45 μm filter (Nylon 66, China). The filtrate was then applied onto a reverse-phase Thermo BDS C18 column (250 mm × 4.6 mm i.d.) (Thermo Fisher Scientific Inc. Waltham, MA) for curcumin quantification. The column, with a particle diameter of 5 μm, was maintained at a temperature of 25 ± 1 °C during the process. The curcumin concentration was determined using an Agilent 1260 Infinity HPLC system (Agilent Technologies, Santa Clara, CA, USA) with a DAD detector operating at 420 nm. The curcumin loading capacity (CLC, μg/mg) was accurately quantified using its peak area by an external calibration curve and expressed as the mass of loaded curcumin (μg) in 1 mg of FSG or HFSG solution.

2.4. SDS-PAGE analysis

Sodium dodecyl sulfate–polyacrylamide gel electrophoresis (SDS-PAGE) analysis was performed with a minor adjustment to reveal the extent of protein hydrolysis according to our previous work (Li et al.,

2021). Briefly, the FSG and $HFSG_{1-2}$ (10 mg) were mixed with a 500 μL SDS solution (4 % SDS, 1 mM DTT, and 150 mM pH 8.0 Tris-HCl), and incubated for 5 min at 45 ℃ with a shaking rate of 120 rpm for 1 h. The sample solution was mixed at a volume ratio of 1:4 (*v/v*) with a loading buffer and then boiled for 5 min before centrifugation (10,000 × g, 3 min). Subsequently, 10 μL of the mixture was carefully loaded into each SDS-PAGE gel well (10 % separating gel and 5 % stacking gel), using the discontinuous tris–glycine buffer (pH 8.3) system (Shanghai Tianneng Technology Co. Ltd., Shanghai, China). The electrophoresis process was carried out by a DYCZ-24KS electrophoresis cell (Beijing Liuyi Biotechnology Co., Ltd., Beijing, China). The initial voltage of the electrophoresis instrument was 80 V. After the marker strips were separated, the voltage was adjusted to 120 V until the blue lane extended to the base bottom. The gel was stained by an aqueous solution with 0.1 % (*w/v*) Coomassie Brilliant Blue R-250 for 1 h. The gel was subsequently destained with 30 % (*v/v*) methanol and 10 % (v/v) acetic acid. The treated gel was imaged with a scanner (i800 Plus, Microtek, Shanghai, China). A prestained protein ladder (10–310 kDa, Thermo Fisher, Waltham, MA, USA) was used to estimate the molecular weight of the sample.

2.5. Determination of surface hydrophobicity of FSG and HFSG

Surface hydrophobicity was determined according to the hydrophobic chromophore bromophenol blue (BPB) method reported by (Bertsch, Mayburd, & Kassner, 2003). The samples (1 mL) were mixed with 200 μL of 1 mg/mL BPB. The solution was then vortexed for 10 min at 25 ℃ after continual shaking and centrifuged at 8,000 × g for 10 min. The obtained supernatant was diluted 10-fold with deionized water and the absorbance of the supernatant (A) was measured at 595 nm using an ultraviolet–visible spectrophotometer against a distilled water blank. A sample subjected to the same treatment but without the protein suspension was used as the control. The hydrophobicity results were expressed as the amount of BPB bound to the protein (BPB_{bound}).

$$BPB_{bound/\mu g} = \frac{200\ \mu g \times (A_{control} - A_{sample})}{A_{control}} \quad (1)$$

2.6. Determination of M_w of FSG and $HFSG_{1-3}$

The FSG, $HFSG_1$ (duration of acid hydrolysis = 1 h), $HFSG_2$ (duration of acid hydrolysis = 3 h) and $HFSG_3$ (duration of acid hydrolysis = 8 h) sample powders were obtained using a vacuum freeze-dryer (10YG/A, SCIENTZ Co., Ltd., Ningbo, China) at −60 °C for 12 h and were then used for subsequent characteristic analysis.

The molecular size distributions of FSG and $HFSG_{1-3}$ were determined with a high-performance size exclusion chromatography (HPSEC) system comprised of a gel column (TSKgel 7.8 x 300 mm G5000PWXL, Tosoh Bioscience GmbH, Griesheim, Germany), and an RI detector (10A, Shimadzu, Japan) (Lazaridou, Biliaderis, & Izydorczyk, 2003). The flow rate of the mobile phase (0.02 % NaN_3), which was filtered through a 0.2 mm cellulose acetate membrane, was 0.5 mL/min; chromatography was performed at 40 ℃. The calculation of the apparent M_w for the samples was based on calibration with glucan standards (M_w of 4×10^3, 7×10^3, 50×10^4, 100×10^4, and 200×10^4 g/mol). The calibration curve of these standard samples is provided in the supplementary material (Fig. S1).

2.7. Amino acid analysis of FSG and $HFSG_{1-3}$

The amino acid composition was determined by subjecting FSG to acid hydrolysis for varying durations. 6 M HCl was added to a glass hydrolysis tube containing 150 mg each of FSG or $HFSG_{1-3}$ and the mixture was degassed for 30 min. Subsequently, the tubes were sealed using nitrogen and placed in an oil bath for hydrolysis at 110 ℃ for 24 h. After hydrolysis, the solution was filtered and diluted with distilled water into a 50 mL volumetric flask and transferred into a glass bottle. To fully dissolve the samples, 1.0 mL of 0.02 M HCl was added, followed by a deacidification step at 45 ℃ using a rotary evaporator (Jingyi Xingye Technology Co., Ltd., Xiamen, China). Following this, 2.0 mL of samples, diluted with sodium citrate buffer, were filtered through a 0.45 μm nylon membrane. The amino acid composition was then analyzed using an automatic amino acid analyzer (A300, membraPure GmbH, Germany). The amino acid contents were quantified using the external standard method as described by Lamp, Kaltschmitt, and Lüdtke (2018). The results are expressed as the proportion of each amino acid to the total amino acids (mg/g).

2.8. Circular dichroism spectroscopy (CD) analysis

The CD spectra of the samples (0.5 mg/mL) dissolved in 10 mM PBS (pH = 7) were analyzed with a spectropolarimeter (JASCO J-815, JASCO Co., Ltd., Tokyo, Japan). Scanning was carried out in the far-UV range of 190 – 250 nm with an interval of 1 nm. The secondary structure compositions (α-helix, β-sheet, β-turn, random coil) were calculated using the DICHROWEB software.

2.9. Measurement of the intermolecular interactions of FSG and $HFSG_{1-3}$

The samples were treated with protein-denaturing chemicals selected for their capacity to disrupt certain kinds of interactions between molecules according to the method of Yang, Su, & Li (2020). Sodium chloride solution (0.6 mol/L) was used to disrupt ionic bonds, 1.5 mol/L urea was used to disrupt hydrogen bonds, 8 mol/L urea simultaneously disrupted hydrogen bonds and prevented hydrophobic interactions, and 0.5 mol/L β-mercaptoethanol disrupted disulfide bonds. The four selected solvents were: 0.6 mol/L sodium chloride solution (SA), 0.6 mol/L sodium chloride solution + 1.5 mol/L urea (SB), 0.6 mol/L sodium chloride solution + 8 mol/L urea (SC), 0.6 mol/L sodium chloride solution + 8 mol/L urea + 0.5 mol/L β-mercaptoethanol (SD). Samples were respectively dissolved in the four selected solvents to analyze the contribution of different interactions in the process of forming FSG with or without acid-induced hydrolysis. The differences in gel solubility in different solvents (i.e. SB, SB-SA, SC-SB, and SD-SC) were used to indicate the contribution by ionic bonds, hydrogen bonds, hydrophobic interactions, and disulfide bonds, respectively. These four mentioned interactions are responsible for maintaining the FSG structure during acid-induced hydrolysis. The samples (100 mg) were homogenized with 10 mL of each solvent in a homogenizer (IKA T18 basic, IKA-Werke GmbH & Co., Staufen, Germany) for 2 min at 12,000 rpm and then centrifuged (8000 × g, 4 ℃, 15 min). The protein concentration in the supernatant was determined using a Pierce™ Coomassie Plus Bradford assay kit (No. 23238, Thermo Fisher Scientific). Results were expressed as mg soluble protein/mL of homogenate.

2.10. Characterization of FSG and $HFSG_{1-3}$ with and without curcumin loading

2.10.1. Fourier transform-infrared spectroscopy (FT-IR)

FTIR spectra were performed on the FTIR 2000 spectrophotometer (Perkin-Elmer, Norwalk, CT, USA) with a deuterated triglycine sulfate detector. The spectra were collected in a range of 4000 – 500 cm^{-1} with a resolution of 4 cm^{-1}, using 32 scanning times at ambient temperature. Dry air was taken as a reference.

2.10.2. X-ray diffraction (XRD)

The XRD patterns (from 6- to 30°) of samples were depicted using an X-ray polycrystalline powder diffractometer (D8 ADVANCE, Brugger, Germany). Measurements were carried out at 40 kV and the scanning rate was 2°/min. The scanning result was analyzed by Jade 5.0 software. The crystallinity indices (CrI%) of FSG and $HFSG_{1-3}$ were calculated

using the following equation (Hao et al., 2015):

$$(\mathrm{CrI}\%) = \frac{100(I_{Max} - I_{Am})}{I_{Max}} \quad (2)$$

I_{Max} here had a maximum intensity of 14.9° and I_{Am} featured an intensity of diffraction for the amorphous region at 2θ = 19.4°.

2.10.3. X-ray photoelectron spectroscopy (XPS)

XPS experiments were conducted using an XPS spectrometer (Scientific K-Alpha, Thermo, USA) with an Al Kα X-ray source (HV = 1486.6 eV) to investigate the chemical state of atoms on the surface of the samples. The energy standard of C_{1s} (284.80 eV) was used for charge correction. Survey spectra were recorded over 0 – 1,350 eV binding energy range at a step size of 1 eV and detector pass energy of 280 eV.

2.10.4. Particle size, ζ-potential, and polydispersity index (PDI) measurements

The mean particle diameter (Z-average), polydispersity index (PDI), and ζ-potential were determined using a combined dynamic light scattering and particle electrophoresis instrument (Nano-ZS 90, Samufei instruments, USA) (Huang et al., 2019). Specifically, the characterization of the particles, expressed as the cumulative mean diameter (size, nm) and the polydispersity index (PDI), were derived by applying the intensity-weighted diameter calculation based on the Stokes-Einstein equation. For the determination of the ζ-potential, an electrophoretic mobility measurement was carried out using the Smoluchowski model (Dai, Reichert, Hinrichs, & Weiss, 2019). Before analysis, the freshly prepared sample solutions were diluted with 1 mg/mL PBS buffer (10 mM, pH 7.2) to minimize the multiple scattering effect. All measurements were carried out at 25 ± 0.5 ℃.

2.11. Microstructure observation

2.11.1. Transmission electron microscopy (TEM) observation

The sample morphology was imaged by TEM (JEM 1200EX, JEOL, Japan) (Liu et al., 2013). The freshly prepared samples were diluted to 0.5 mg/mL with deionized water. One drop of the diluted sample was then placed on a 400-mesh copper grid and stained with 1 % phosphate tungsten for 30 s. The images were obtained with a Tungsten filament lamp at 80 kV.

2.11.2. Confocal laser scanning microscopy (CLSM)

The distribution of the curcumin-loaded nanoparticles within the FSG and HFSG was observed by CLSM (Leica TCS SP8). The measurement of curcumin nanoparticles was carried out at excitation and detection wavelengths of 405 nm and 470 – 556 nm, respectively. The measurements of rhodamine B-labeled FSG and HFSG were performed at excitation and detection wavelengths of 570 nm and 565 – 685 nm, respectively.

2.12. In-vitro digestion behavior

Simulated gastric fluid (SGF) and intestinal fluid (SIF) were prepared following the detailed method provided by Yu et al. (2022). The concentration of the control sample (free curcumin) was measured to 21 μg/mL and dissolved in a solution containing 25 % dimethyl sulfoxide (DMSO). The determination of the curcumin stability was as follows: the sample and simulated gastrointestinal fluid were mixed at a ratio of 1:4 and shaken on a vortex mixer for 1 min. The mixed solution was then placed in a constant temperature shaking incubator (120 r/min, 37 °C). Samples of 3.0 mL were withdrawn at intervals of 10-, 20-, 30-, 40-, 60-, and 90 min for SGF and, to account for the extended period in simulated intestinal digestion, SIF was withdrawn at intervals of 10-, 30 min and 1-, 2-, 4-, and 6 h. The curcumin concentration of the samples was quantified following the method described in Section 2.5. The retention rate of curcumin was calculated as the ratio of the curcumin content at a specific duration compared to the initial curcumin content. On the other hand, the method for measuring the distinct release rate of curcumin was as follows: by dissolving 100 mg of both CL-FSG and CL-$HFSG_2$ in 10 mL of distilled water, the resulting solution of 3.0 mL was added to a test tube and then transferred into a dialysis bag. This mixture was subsequently incubated in 50 mL of simulated gastrointestinal fluid and subjected to magnetic stirring at 37 °C. 1.0 mL of the external fluid from the dialysis bag was extracted at the aforementioned specific digestion time. The formula employed for calculating the release rate of curcumin was as follows:

$$Curcuminreleaserate(\%) = \frac{C_t \times 50}{C_0 \times 3} \times 100 \quad (3)$$

Where C_t is the curcumin concentration in the fluid external to the dialysis bag at a particular time interval, while C_0 is the curcumin concentration within the dialysis bag. The values 50 and 3 refer to the volumes of the external and internal fluids of the dialysis bag, respectively.

The bioaccessibility and bioavailability were calculated as follows:

$$Bioaccessibility(\%) = \frac{C_{micelle}}{C_{digesta}} \times 100 \quad (4)$$

$$Bioavailablibility(\%) = \frac{C_{micelle}}{C_{initial}} \times 100 \quad (5)$$

Where $C_{initial}$, $C_{micelle}$ and $C_{digesta}$ are the content of curcumin in initial samples, micelle fractions, and overall digestates at the end of the simulated gastrointestinal digestion.

2.13. Statistical analysis

Results were expressed as the mean with a standard deviation from at least three measurements. SPSS 20.0 was used to analyze the data. The one-way analysis of variance (ANOVA) was performed to determine the least significance at $P < 0.05$ by Tukey's HSD test. All graphics were plotted using Origin software 2018 (Origin Lab Corp., MA, USA).

3. Results and discussion

3.1. Effect of duration of acid hydrolysis on the molecular weight (M_w) and CLC (curcumin loading capacity, μg/mg) of FSG and acid-hydrolyzed FSG (HFSG)

The determination of the dissolved curcumin content in an aqueous solution provides crucial evidence indicating the effectiveness of nanoparticles as carriers for hydrophobic molecules. Fig. 1 (A) shows that FSG loaded a minimal amount of curcumin into its neutral hydrophobic region without acid treatment. This amount of curcumin probably resulted from the presence of several hydrophobic amino acids (such as phenylalanine, proline, and alanine) in FSG (Table. S1), although the aqueous extract of gelatin from FS is overwhelmingly composed of a hydrophilic backbone. The hydrophobic interaction between the curcumin and the hydrophobic amino acid residues of the FSG led to a curcumin concentration of only 2.16 ± 0.13 μg/mL, as the interior structure of FSG unfolded after the solubilization. The curcumin concentration in FSGH at the initial stage was noticeably higher than that in the FSG. A pronounced increase in curcumin concentration from 6.06 ± 0.36 to 18.30 ± 0.38 μg/mL was observed when acid hydrolysis was prolonged from 1 h to 3 h. However, it is important to note that during phase 2 of acid hydrolysis (3 – 8 h), the curcumin concentration in acid-hydrolyzed FSG did not exhibit a continuous increase with extended acid hydrolysis. Contrariwise, there was a significant decrease in the curcumin concentration ($P < 0.05$). The curcumin concentration showed a slight variation within the range of 2.15 ± 0.38 to 3.72 ± 0.57 μg/mL. This phenomenon can be attributed to excessive hydrolysis,

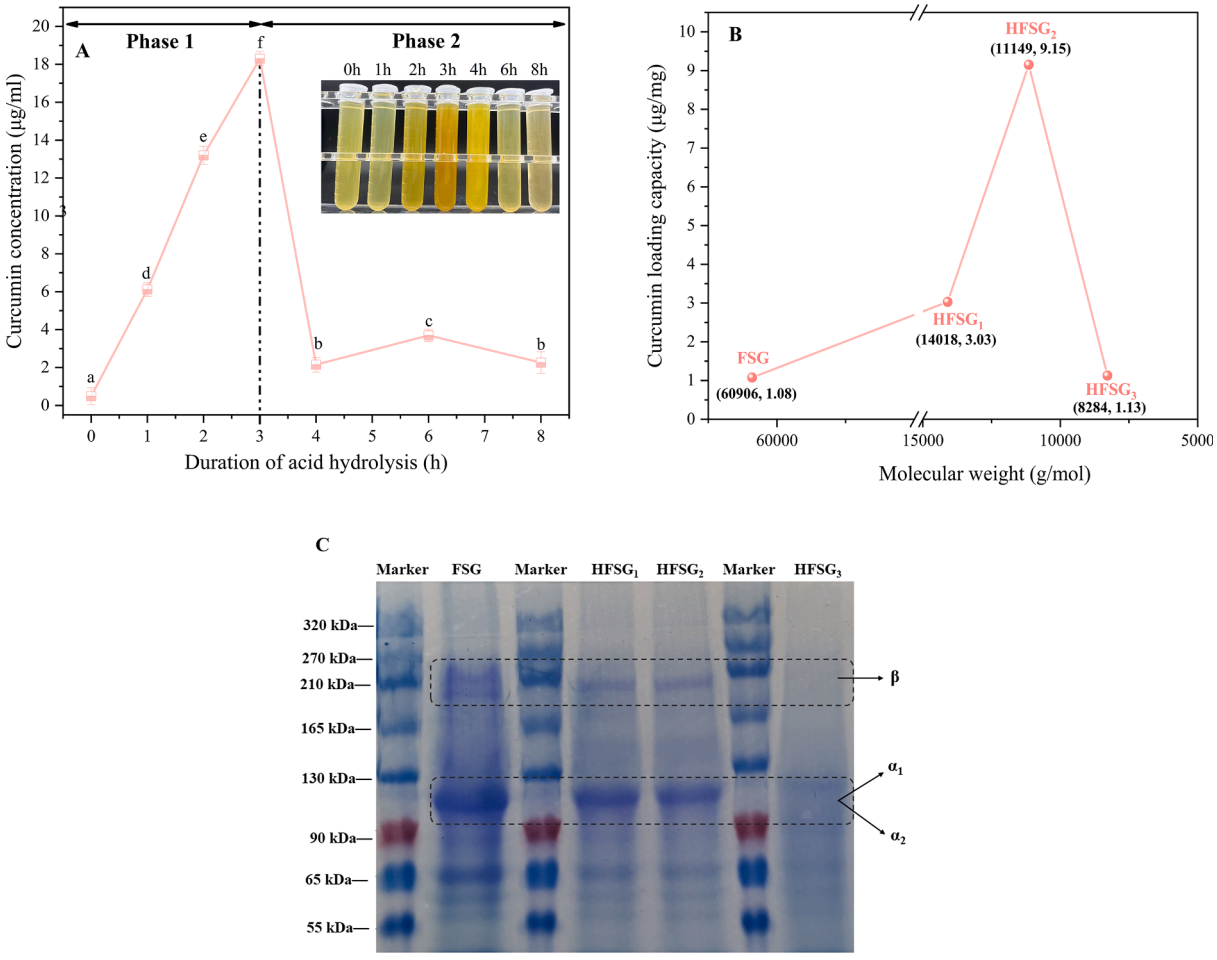

Fig. 1. Curcumin concentration (μg/mL) of FSG with 0 – 8 h acid hydrolysis (A), curcumin loading capacity (CLC, μg/mg) of HFSGs having different molecular weights and durations of acid hydrolysis (B), and SDS-PAGE patterns of FSG and HFSGs ($HFSG_1$, duration of acid hydrolysis = 1 h; $HFSG_2$, duration of acid hydrolysis = 3 h; $HFSG_3$, duration of acid hydrolysis = 8 h) (C). Values in bearing different lowercase letters are significantly different ($P < 0.05$).

which hinders the formation of hydrophobic regions within the molecule (Dai, Reichert, Hinrichs, & Weiss, 2019).

On the other hand, the CLC (μg/mg) for FSG and $HFSG_{1\text{-}3}$ with different M_w is summarized in Fig. 1 (B). The acid treatment of FSG caused significant degradation in the M_w of FSG from 60,906 (0 h) to 14,018 (1 h), 11,149 (3 h) and 8,284 (8 h) g/mol respectively. Gelatin readily undergoes degradation in an acidic pH environment (Huang et al., 2019). Given the above results, it can be inferred that a further decrease in gelatin M_w would give rise to an increase in molecular mobility, which would impede the formation of intramolecular hydrophobic regions (Acevedo et al., 2017).

3.2. *Effect of duration of acid hydrolysis on the characteristics of FSG and HFSG*

3.2.1. *Effect of duration of acid hydrolysis on the amino acid and molecular weight compositions of HFSG*

The amino acid compositions of FSG and $HFSG_{1\text{-}3}$ are presented in Table S1. Tryptophan was not detected because it was destroyed during acid hydrolysis, and glutamine and asparagine were also converted to glutamate and aspartic acid (He et al., 2021). The amino acid components can be easily acquired through acid hydrolysis and dissolution. The quantity of these components gradually decreased, resulting in a significant reduction in the total amino acid (TAA) content of HFSG compared to FSG (Li et al., 2024). Following acid hydrolysis, the TAA content in HFSG exhibited a remarkable reduction compared to FSG (from 524.2 mg/g to 229.3 ~ 268.9 mg/g), which can be ascribed to acid hydrolysis. In terms of the ratio of HAA to AA, a slight increase was observed from 41.1 % (0 h) to 48.2 % (1 h) and 49.1 % (3 h) due to the prolongation of acid hydrolysis, while further acid hydrolysis did not lead to a continuing increase in the ratio of HAA to TAA. It can be inferred from the increased HAA of $HFSG_2$ that moderate acid treatment facilitated the unfolding of FSG, exposing hydrophobic groups and regions inside the molecule to make it more suited for constructing advanced, self-assembled nanoparticles as promising carriers for curcumin loading.

The SDS-PAGE technique was employed to analyze the molecular weights of FSG and $HFSG_{1\text{-}3}$, their subunit compositions, and their hydrolysates at different stages of hydrolysis. The protein components of the FSG and $HFSG_{1\text{-}3}$ with different molecular weight distributions are depicted in Fig. 1 (C). The FSG presented a typical molecular weight (M_w) distribution for fish gelatin, with distinct electrophoretic bands corresponding to α-chains (α_1 and α_2, 130 – 100 kDa) and β-chains (~210 kDa) (Li et al., 2021). Moreover, proteins at $M_w < 100$ kDa (including 90, 65, 55 kDa) were readily detected in the FSG. Protein molecules with molecular weights < 100 kDa consisted of degraded collagen chains and residues of non-collagenous proteins (Nitsuwat et al., 2021). This phenomenon comports with previous research that extracted gelatin from bighead carp scales using ultrasound treatment (Yang, Su, & Li, 2020). The distinct bands of α_1, α_2, and β-chains revealed visibly weakened staining with the prolongation of the acid hydrolysis. Some larger subunits were dissociated into smaller subunits, indicating that acid hydrolysis resulted in the dissociation of gelatin. Notably, when the duration of the acid hydrolysis extended to 8 h, no

subunits were observed in the electrophoretic pattern for $HFSG_3$, indicating excess acid hydrolysis of the subunits. To clarify the exact extent of hydrolysis, it was quantified by calculating the protein content ratio, specifically referred to as the protein retention rate, in the freeze-dried samples of untreated FSG and HFSG subjected to varying degrees of acid hydrolysis. As the acid hydrolysis duration extended from 1 h to 8 h, the protein retention rates of $HFSG_1$, $HFSG_2$, and $HFSG_3$ decreased from 84.2 % to 73.68 % and 68.42 %, respectively. Coupled with the molecular weight distribution results (Fig. S2), it can be inferred that the prolonged acid hydrolysis, which induced excessive degradation of the gelatin molecules, gradually reduced the molecular weight of HFSG, thereby resulting in the loss of recoverable protein.

3.2.2. *Analysis of secondary protein structural composition, intermolecular interactions, and surface hydrophobicity among FSG and $HFSG_{1-3}$*

Circular dichroism (CD) spectrometry was used to analyze the secondary structure of proteins and to illustrate the conformational transition from FSG to HFSG. The CD spectra of FSG and $HFSG_{1-3}$ generally have a negative absorption peak at 190 – 210 nm representing the random curl of gelatin molecules with a typical absorption peak near 230 nm, corresponding to the twisted antiparallel β-sheet of the gelatin as shown in Fig. 2 (A) (Gopal, Park, Seo, & Park, 2012). The secondary structural composition of FSG and HFSG is recorded in Fig. 2 (B). It was shown that compared to FSG, the relative content of α-helix and β-turn in $HFSG_2$ decreased by 61.7 % and 11.9 %, respectively, while there was a substantial increase of 47.6 % in the content of β-sheet. The results indicated that acid treatment during the early stage (0 – 3 h) promoted the unfolding and rearrangement of the α-helix structure of FSG into a β-sheet. This process was followed by the self-assembly of FSG into nanoparticles, with a hydrophobic layer formed in the center of the nanoparticles. The hydrophobic region collapsed to reduce hydrophobic domain interactions with water, thus the hydrophobic core was able to retain the hydrophobic curcumin molecules (Yu et al., 2022). Subsequently, the curcumin was encapsulated within the assembled network. This observation demonstrated that $HFSG_2$ had superior curcumin loading capacity. However, with the prolongation of acid hydrolysis of FSG, $HFSG_3$ showed a slight decrease in relative β-sheet content and an increase in random coils, inferring that excessive acid hydrolysis of FSG might destabilize the hydrophobic domains between protein molecules.

In the process of the acid hydrolysis of FSG, acidification altered the forces that maintained the complex protein structure, and new intermolecular forces formed to stabilize the gel structure during the denaturation and reaggregation of the protein. The main driving force in the network formation and structuring of HFSG, however, is unclear. The ionic bonds, hydrogen bonds, hydrophobic interactions, and disulfide bonds of FSG and FSG hydrolysate were thus determined. As depicted in Fig. 2 (C), unmodified FSG has stronger ionic bonds and hydrogen bonds as compared with disulfide bonds and hydrophobic interactions, suggesting that ionic bonds and hydrogen bonds are the key driving forces maintaining the natural structure of FSG. After the self-aggregation of FSG induced by acid hydrolysis, however, the contribution by hydrogen bonds and ionic bonds diminished; in contrast, the hydrophobic interactions and disulfide bonds displayed an opposite trend. More specifically, the percentage contributions of ionic bonds and hydrogen bonds decreased by 33.61 ~ 38.72 %, 16.52 ~ 29.81 %, respectively, while the percentage contributions of hydrophobic interactions and

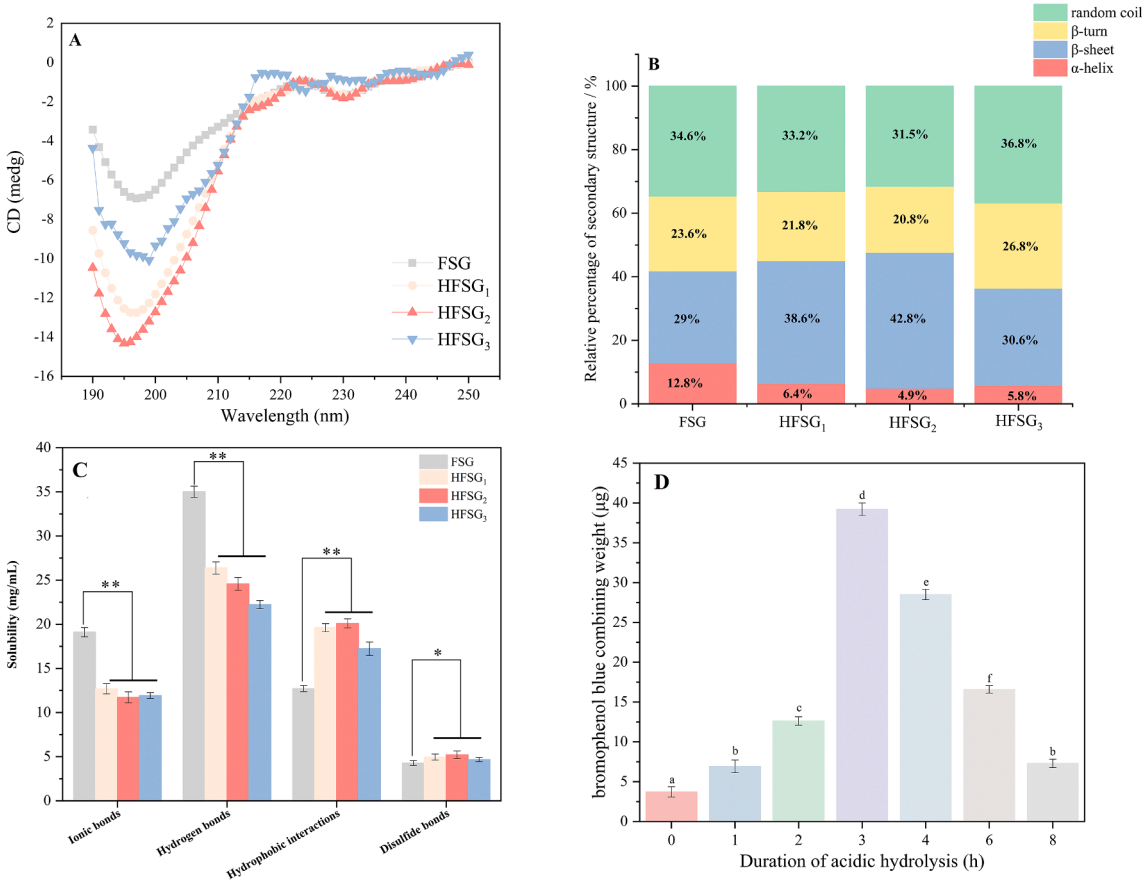

Fig. 2. CD spectra (A) and their relative content of secondary structure of FSG during acid treatment process (B), intermolecular interactions of FSG and HFSGs (including $HFSG_1$, duration of acid hydrolysis = 1 h; $HFSG_2$, duration of acid hydrolysis = 3 h; $HFSG_3$, duration of acid hydrolysis = 8 h) (C) and the effect of the duration of acid hydrolysis on the surface hydrophobicity of FSG (D). The "*" represents a significant correlation at the 0.05 level, "**" represents a significant correlation at the 0.01 level.

disulfide bonds increased by 35.53 ~ 58.06 % and 9.36 ~ 22.02 %, respectively. The reduction of ionic bonds and hydrogen bonds during acid hydrolysis may relate to the binding and aggregation of FSG under acid-induced treatment (as implied in TEM and CLSM results). The native structure of FSG was changed owing to the weaker hydrogen and ionic bonds, which led to a change in the molecular structure of FSG. Additionally, it is worth noting that acid hydrolysis in the first three hours facilitated the unfolding of FSG molecules, exposing numerous hydrophobic groups to form hydrophobic aggregates, thus substantially enhancing the hydrophobic interactions. However, with the prolongation of further acid hydrolysis of FSG (8 h), the hydrophobic interactions were subsequently weakened. The disulfide bonds increased slightly; the formation of disulfide bonds being caused by oxidation of the sulfhydryl groups embedded in the FSG. The relatively higher composition of sulfur-containing amino acids (Met and Cys) in $HFSG_2$ compared to $HFSG_1$ and $HFSG_3$, as shown in Table S1, substantially accelerated the formation of disulfide bonds. Similar results were found in soybean gel modified by *Lactobacillus plantarum*, which was stabilized by hydrophobic interactions and disulfide bonds (Yang, Su, & Li, 2020). Thus, it could be concluded that hydrophobic interactions and

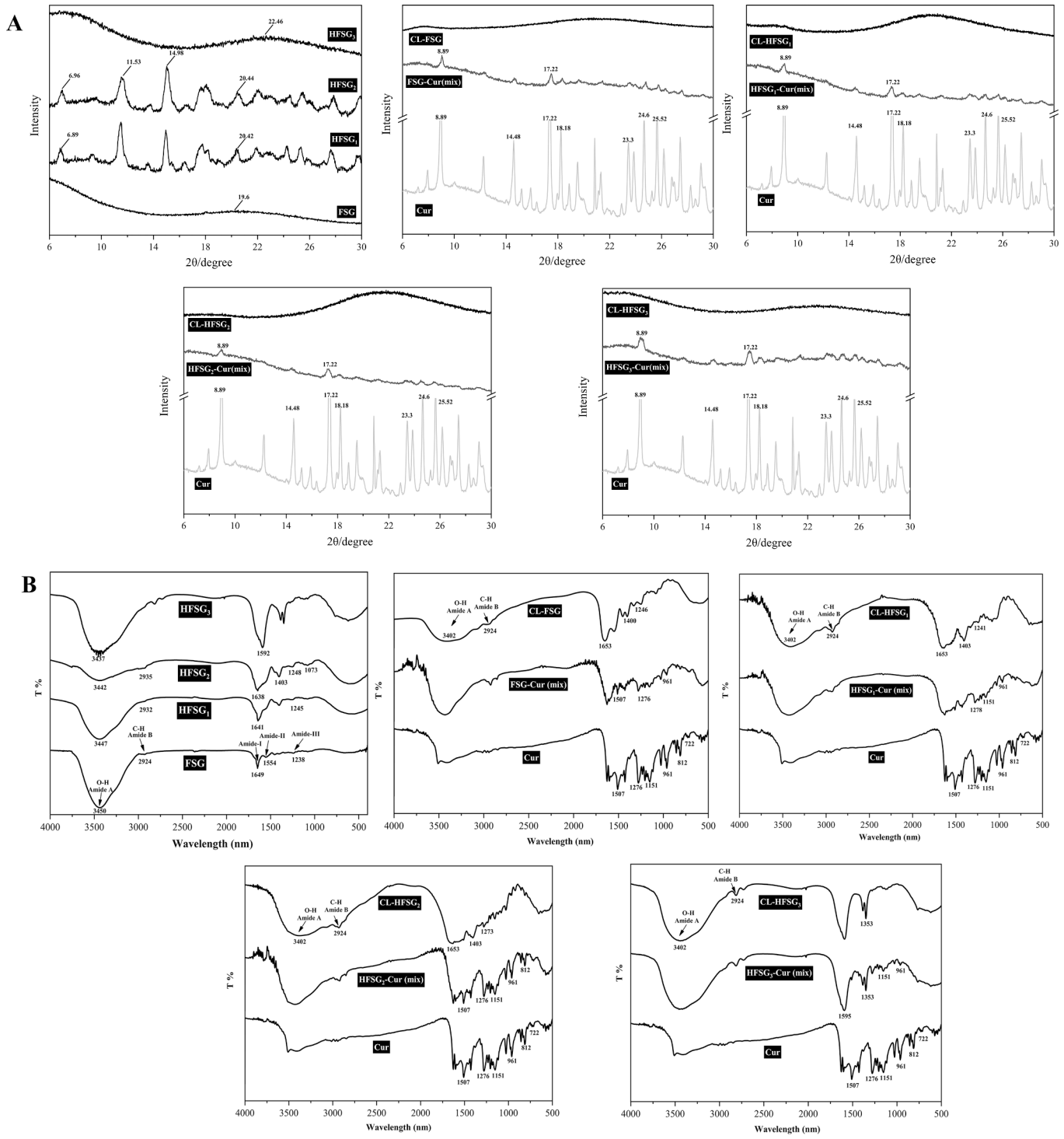

Fig. 3. X-ray diffraction (XRD) (A) and Fourier Transform infrared spectroscopy (FTIR) (B) of FSG and HFSGs ($HFSG_1$, duration of acid hydrolysis = 1 h; $HFSG_2$, duration of acid hydrolysis = 3 h; $HFSG_3$, duration of acid hydrolysis = 8 h) with or without the loading of curcumin and mixtures of curcumin and samples.

disulfide bonds are the primary chemical forces maintaining the stable conformation of acid-induced FSG.

Changes in surface hydrophobicity can be regarded as a useful tool to assess changes in the exposure of the hydrophobic regions in the protein and aggregation via the distribution of hydrophobic groups on the gelatin surface (Ji et al., 2023). As shown in Fig. 2 (D), the surface hydrophobicity of FSG increased significantly at the initiation of acid hydrolysis and then decreased and finally leveled off with the prolongation of acid hydrolysis. After three hours of treatment, FSG exhibited the highest surface hydrophobicity, with a binding capacity for bromophenol blue that was tenfold greater than that of untreated FSG. The results showed that an appropriate degree of acidic treatment effectively denatured FSG, promoting the unfolding of gelatin and exposing its buried hydrophobic groups. This process provides optimal conditions for particle aggregation through hydrophobic forces. The higher surface hydrophobicity of $HFSG_2$ aggregates emerged due to increased hydrophobic interactions. However, with the further prolongation of acidic treatment, the surface hydrophobicity of HFSG showed the opposite tendency. Decreased surface hydrophobicity caused the aggregation of HFSG, resulting in partially blocking hydrophobic cavities or fissures on the surface of HFSG molecules (Linden & Venema, 2007). The decrease in surface hydrophobicity may also be ascribed to the proteins being shielded by negative charges (Du et al., 2022). Moreover, a deamidation reaction converts the hydrophobic side chain groups of some glutamine residues into carboxyl groups, reducing the hydrophobic FSG binding sites for bromophenol blue (Yang, Su, & Li, 2020).

3.3. Characterization of FSG and $HFSG_{1-3}$ with or without the loading of curcumin

3.3.1. XRD analysis

XRD analysis was used to elucidate alterations in the crystalline or amorphous structures of native and acid-hydrolyzed FSG, either in the presence or absence of curcumin loading, and mixtures of curcumin and samples. According to the report from Sha et al. (2014), the two characteristic peaks of fish gelatin were found in the range of 6 – 9° and 17 – 21.5° and indicated the triple-helical structure and the single, left-hand helical chain, respectively. The intensity of the diffraction peaks reflected the respective number of triple helical strands. However, FSG displayed only one characteristic diffraction peak at near 19.6° as shown in Fig. 3 (A). This observation might be ascribed to the destruction of the triple helical structure in FSG after the high-temperature extraction process. This suggested that an ordered state of FSG formed during the process of acid hydrolysis, which caused two sharp diffraction peaks to appear in the spectra of $HFSG_1$ (6.89° and 20.42°) and $HFSG_2$ (6.96° and 20.44°). Furthermore, the peak intensity of the sample treated with acid hydrolysis gradually increased at the initial stage (0–3 h) with the prolongation of acid hydrolysis. At the same time, in the first stage of acid treatment, two noticeable diffraction peaks 2θ emerged for $HFSG_{1-2}$ at 11.53° and 14.98°. This may be due to the fact that strong forces induced a conformational change in the FSG structure, which led to structural aggregation and produced a strong diffraction peak. In addition, the crystallinity was determined in order to delve deeper into the effect of acid hydrolysis on the structural features of FSG; the values were 5.52 %, 26.55 % and 30.82 %, for FSG, $HFSG_1$, and $HFSG_2$, respectively. The increased crystallinity might be attributed to acid hydrolysis, which facilitated the dissolution of the amorphous area in $HFSG_{1-2}$. With the acid treatment extended to 8 h, the ordered triple helix structure reverted to the amorphous state with a crystallinity value of 12.61 %. This reversion might be ascribed to weaker hydrophobic interactions without sufficient hydrogen bonding between glycine and proline to maintain the triple helix of FSG, which is in line with our amino acids results.

On the other hand, the characteristic peaks of curcumin at 8.89°, 14.48°, 17.22°, 18.18°, 23.3°, 24.60° and 25.52° indicated that curcumin is a highly crystalline compound with a relative crystallinity up to 92.1 %. Weak absorption peaks at 8.89° and 17.22° were found in the mixture of curcumin, FSG together with $HFSG_{1-3}$, indicating that a crystalline state of curcumin still exists in the mixture of curcumin and FSG with or without acid treatment. Noticeably, after loading curcumin into FSG or $HFSG_{1-3}$, a broad peak was observed only in the XRD spectra between 18° to 27°, the curcumin XRD diffraction patterns of disappeared completely after being encapsulated by these nanoparticles, which indicated that the encapsulation changed the molecular arrangement of the samples and the physical properties of curcumin from a crystallized state to an amorphous state. It has been consistently reported that bioactive substances will have their crystalline structure disappear after being encapsulated, resulting in the amorphous states having higher internal energy and being conducive to the absorption and utilization of curcumin (Liang et al., 2023).

3.3.2. FT-IR analysis

As depicted in Fig. 3 (B), the spectra of unmodified FSG contain a broad band at 3,450 cm^{-1}, resulting from amide A (3,100–3,500 cm^{-1}), which is caused by the stretching vibration of the –OH group coupled with hydrogen bonding (Wang, Williams, & Senan, 2014). The peak intensity of $HFSG_{1-3}$ was significantly weaker than that of FSG, and shifted to 3,447, 3,442, and 3,437 cm^{-1}, respectively, indicating the breakage of interchain hydrogen bonds in FSG, which might be attributed to the limited amide group (–CONH-) content. Electrostatic attractions and hydrophobic interactions were mainly responsible for the diminished peak intensity of $HFSG_{1-3}$. CH_2 stretch bands of $HFSG_{1-3}$ shifted from 2,924 (FSG) to 2,932 ($HFSG_1$), 2,935 ($HFSG_2$) and 2,817 cm^{-1} ($HFSG_3$), stemming from amide B (2,800–3,000 cm^{-1}), inferring that hydrophobic interaction was enhanced and then attenuated after acid hydrolysis. Moreover, FTIR spectra of FSG showed characteristic amide-I (1,600–1,700 cm^{-1}), amide-II (1,500–1,600 cm^{-1}) and amide-III (1,220–1,330 cm^{-1}) bands at approximately 1,633, 1,554 and 1,237 cm^{-1} (Uriarte-Montoya et al., 2011). The peak of FSG at 1649 cm^{-1} refers to amide I (1,600–1,700 cm^{-1}) and derives from the stretching vibrations of the C═O and C—N groups (Sow & Yang, 2015). The peak of FSG at 1,554 cm^{-1} represents amide II and derives mainly from the C—N tensile vibration coupled with in-plane N—H bending modes, and C—C stretching vibrations (Yu et al., 2022). The peak of FSG at 1,238 cm^{-1} refers to amide III and is mainly ascribed to C—N tensile vibration, N—H deformation of the amide bond, and the swinging vibrations of glycine and proline CH_2 groups. In addition, the peak position of amide III for $HFSG_{1-3}$ showed a pronounced shift from 1,238 (FSG) to 1,245 ($HFSG_1$), to 1,248 ($HFSG_2$) and to 1,250 cm^{-1} ($HFSG_3$), respectively, implying that acid treatment altered the C—N or N—H bond of FSG. Moreover, a new absorption peak was found at 1,403 cm^{-1} in $HFSG_{1-3}$, which is the *cis*-configuration represented by the $HFSG_{1-3}$ absorption peak, characterizing the peptide bond. It can be inferred that the gelatin molecule contains a large proportion of proline (Zhang et al., 2020). This result is consistent with the amino acid results mentioned above. All of the results above indicate that the secondary structure of gelatin changed in the process of acid hydrolysis. In addition, characteristic peaks were observed for curcumin, including those at 722 cm^{-1}, 812 cm^{-1}, 961 cm^{-1}, 1,151 cm^{-1}, 1,276 cm^{-1}, 1,507 cm^{-1}. When mixed with FSG and $HFSG_{1-3}$, the characteristic absorption peak for curcumin remained detectable. Notably, however, after loading curcumin almost all of its characteristic absorption peaks disappeared inside of CL-FSG and CL-$HFSG_{1-3}$ nanoparticles, indicating the successful encapsulation of curcumin. This observation was in line with the results of Li et al. (2021), who reported that the characteristic peaks of curcumin merged or overlapped with the absorption peaks of the polymer matrix upon being loaded in zein/alginate/NaCas nanoparticles.

3.3.3. XPS analysis

XPS was applied to measure the elements and average chemical composition on the surface of the nanoparticles, as it concurrently analyzed the content of surface-embedded substances (Jafari et al.,

2008). Subsequently, we clarified the relationship between the degree of acid hydrolysis and the content of embedded substances on the surface of HFSG. The elemental composition was derived from the atomic binding energy spectra for FSG with or without acid hydrolysis, as depicted in the inset of Fig. 4. The oxygen-carbon ratios observed for FSG, $HFSG_1$, $HFSG_2$, and $HFSG_3$ were 0.206, 0.447, 0.488, and 0.431, respectively, indicating that appropriate acid hydrolysis can prompt the exposure of additional carbonyl groups, consequently creating more binding sites. Such a phenomenon is suggestive of their potential impact on the curcumin loading capacity. With the prolonged duration of the acid hydrolysis, excessive treatment impedes the exposure of hydroxyl groups. This is evidenced by the diminished oxygen-to-carbon ratio and increased nitrogen content in $HFSG_3$, thereby weakening the stability of the core–shell structure. Furthermore, the peak fitting of C_{1s} narrow spectrum using Avantage software yielded insights into the alterations in the surface chemistry of curcumin-loaded HFSG. The peak at approximately 284.8 eV represents C—C and C═C in FSG and curcumin, while the 286.1 eV peak is associated with the carbon atom linked to oxygen in the curcumin molecule's phenolic hydroxyl and methoxy groups (Liang et al., 2023). Peaks 3 and 4 (287.6 – 287.9 eV and 288.7 – 288.9 eV, respectively) correspond to –C═O and –C═O–O (Shi, Kokini, & Huang, 2009). Based on the data presented in the inset of Fig. 5, CL-FSG and CL-HFSG exhibit distinct mechanisms for curcumin loading. In the case of CL-FSG, curcumin is adsorbed onto nanoparticles. While in CL-HFSG, curcumin predominantly accesses the hydrophobic cavity through the core–shell structure formed by HFSG nanocarriers. The proportion of curcumin characteristic groups on CL-HFSG surfaces was 21.86 % ($HFSG_1$), 20.17 % ($HFSG_2$), and 23.85 % ($HFSG_3$). With the extension of acid hydrolysis duration, there is an initial increase followed by a subsequent decrease in the efficiency of loading curcumin into the hydrophobic cavity of HFSG nanocarriers. This pattern aligns with the observed curcumin loading capacity of these nanoparticles.

3.4. Self-assembly analysis of FSG and $HFSG_{1-3}$ with or without loading curcumin

Molecular self-aggregation as referred to here is the process by which small molecular units spontaneously organize and form aggregates or supramolecular assemblies with certain structures and function through non-covalent bond interactions (Liu et al., 2022). The self-aggregation of FSG and $HFSG_{1-3}$ with or without the loading of curcumin was characterized using DLS and TEM techniques.

As shown in Fig. 6, TEM reveals a formation of large and polygonous self-assemblies in FSG. Interestingly, in contrast to FSG, the nanoparticle aggregates of HFSG exhibited hollow-core spherical structures, which suggests that enhanced hydrophobic interactions among $HFSG_{1-3}$ led to the alteration of these spherical structures. These structures indicate competition between intramolecular folding and intermolecular aggregate formation. Two charged segments unite through electrostatic attraction, but the resultant nanoparticles are spherical when they come within a distance less than the Debye–Huckel screening length (Saxena, Sachin, Bohidar, & Verma, 2005). After loading curcumin into FSG or HFSG, more hollow-core structures were distributed in CL-$HFSG_{1-2}$. To the contrary, it is evident that, with the prolonged acid hydrolysis, the CL-$HFSG_3$ exhibited a scarcity of hollow-core structures, suggesting excessive acid hydrolysis of FSG impeded the interaction of HFSG with curcumin through hydrophobic interaction.

More details about the particle features detected by DLS are summarized in Table 1. Specifically, particle size, polydispersity index (PDI) and ζ-potential of FSG were 1,362.3 nm, 0.802 and −24.8 mV, respectively. There was a notable reduction in the particle size and PDI from 827.9 nm, 0.626 to 251.5 nm, 0.572, respectively, during the initial

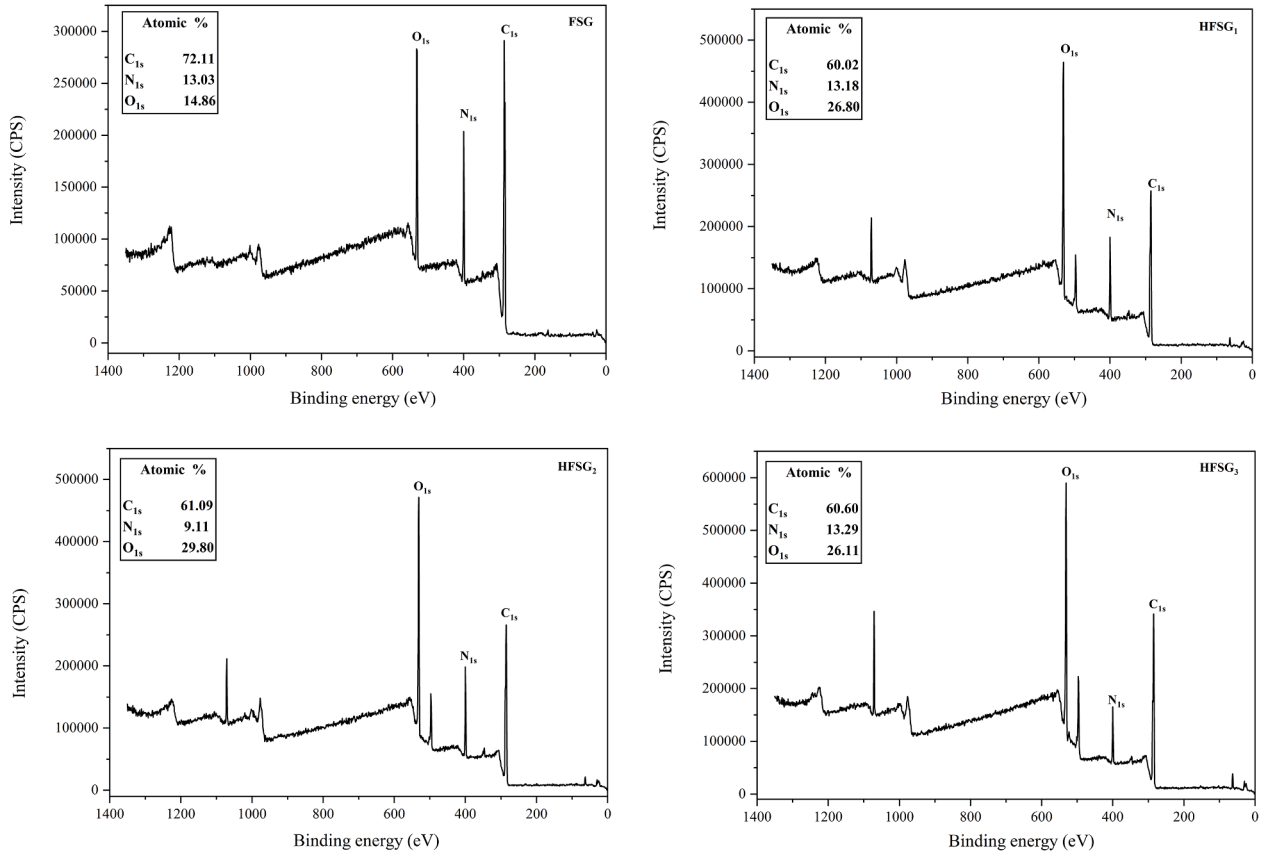

Fig. 4. XPS survey spectra of FSG and HFSGs ($HFSG_1$, duration of acid hydrolysis = 1 h; $HFSG_2$, duration of acid hydrolysis = 3 h; $HFSG_3$, duration of acid hydrolysis = 8 h).

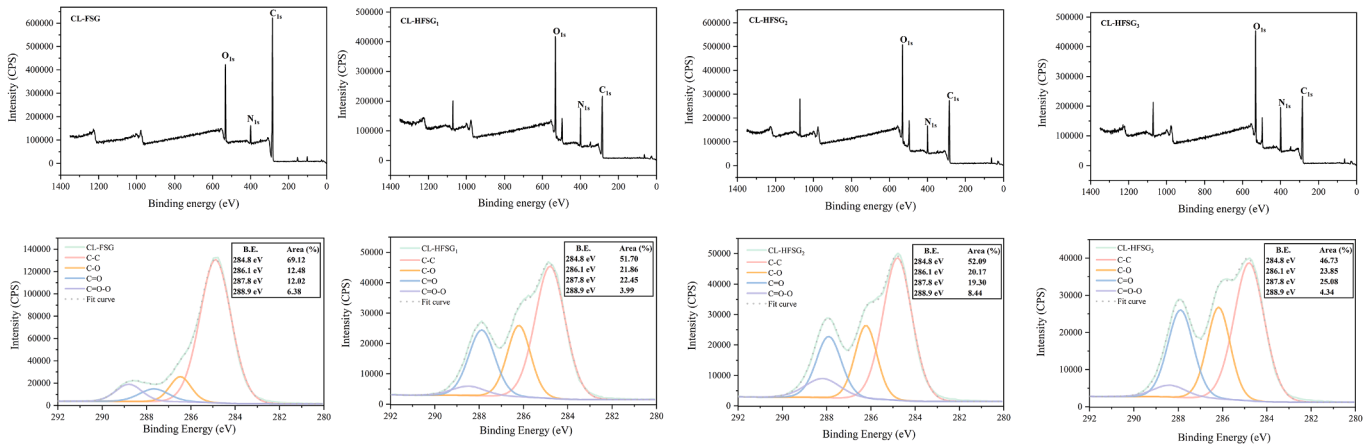

Fig. 5. Atomic binding energy spectra of CL-FSG and CL-HFSGs (curcumin-loaded $HFSG_1$, duration of acid hydrolysis = 1 h; curcumin-loaded $HFSG_2$, duration of acid hydrolysis = 3 h; curcumin-loaded $HFSG_3$, duration of acid hydrolysis = 8 h) and their respective C_{1s} narrow-spectrum peak fitting.

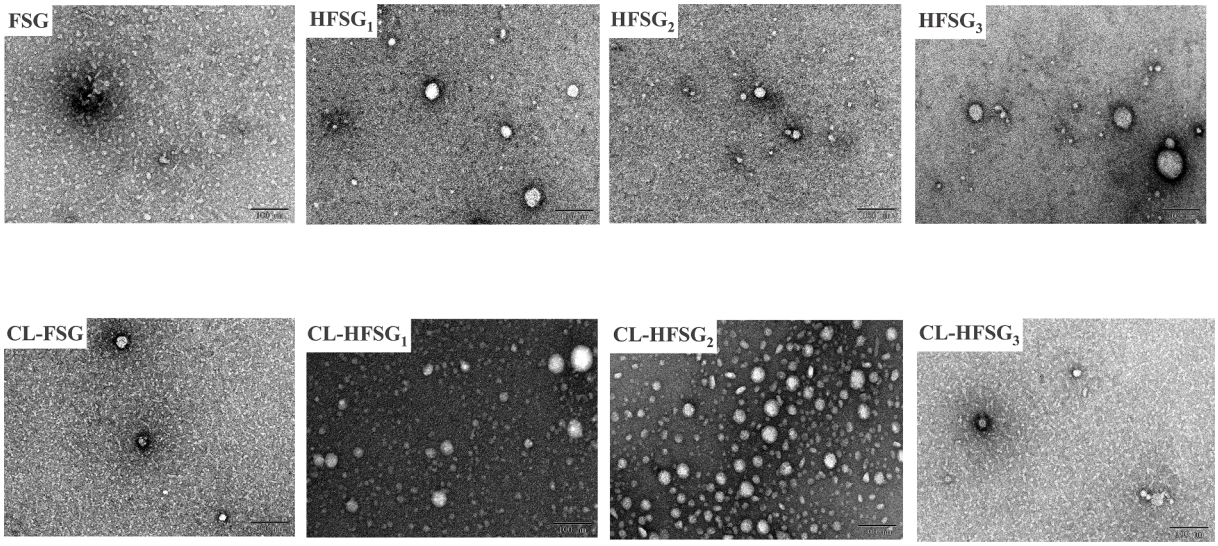

Fig. 6. Transmission electron microscopy (TEM) of fish scale gelatin (FSG) and HFSGs ($HFSG_1$, duration of acid hydrolysis = 1 h; $HFSG_2$, duration of acid hydrolysis = 3 h; $HFSG_3$, duration of acid hydrolysis = 8 h) with or without the loading of curcumin.

Table 1
Particle size, particle distribution index (PDI) and ζ-potential of FSG and $HFSG_{1-3}$ with or without loading curcumin.

Sample	Particle Size (nm)	PDI	ζ-potential (mV)
FSG	1362.3 ± 47.2^{a}	0.802 ± 0.054^{a}	-24.8 ± 0.57^{a}
$HFSG_1$	827.9 ± 23.6^{b}	0.626 ± 0.023^{b}	-5.8 ± 0.39^{d}
$HFSG_2$	251.5 ± 11.4^{f}	0.572 ± 0.017^{c}	-1.4 ± 0.12^{f}
$HFSG_3$	514.3 ± 12.6^{d}	0.682 ± 0.019^{b}	-3.6 ± 0.27^{e}
CL-FSG	668.4 ± 85.7^{c}	0.391 ± 0.054^{d}	-18.6 ± 0.19^{b}
CL- $HFSG_1$	836.8 ± 37.1^{e}	0.604 ± 0.062^{b}	-6.1 ± 0.19^{d}
CL- $HFSG_2$	569.4 ± 67.2^{g}	0.114 ± 0.049^{f}	-8.5 ± 0.85^{c}
CL- $HFSG_3$	290.5 ± 29.3^{f}	0.326 ± 0.034^{e}	-5.7 ± 0.63^{d}

Note: Values of samples bearing different superscript lowercase letters (a, b, c, d, and e) within the particle size, PDI and ζ-potential are significantly different ($P < 0.05$).

three hours of acid hydrolysis. It could be thus inferred that suitable acid hydrolysis promotes the self-assembly of FSG, whereby the intensified hydrophobic interactions contribute to the decrease in both particle size and PDI. However, $HFSG_3$ exhibited pronounced aggregations, culminating in an average particle size of 514.3 nm in the final stage of acid hydrolysis. These undesirable aggregations can be ascribed to excessive acid hydrolysis, possibly resulting in the overexposure of the proteins' hydrophobic regions, and subsequently initiating protein-mediated hydrophobic aggregations. After loading curcumin into FSG and $HFSG_3$, the decrease in particle size and PDI indicated enhanced hydrophobic interactions. This observation follows the results for curcumin-loaded zein nanoparticles (Dai, Reichert, Hinrichs, & Weiss, 2019). In particular, the particle sizes of CL-$HFSG_{1-2}$ were larger when compared to $HFSG_{1-2}$. This is likely attributable to the introduction of curcumin, with its hydrophobicity, prompting neighboring particles to aggregate into larger particles and achieving a solubilizing effect.

The ζ-potential is a critical parameter for analyzing surface properties of self-aggregates and their stability. As depicted in Table 1, ζ-potential increases from −24.8 (FSG) to −5.8 ($HFSG_1$), −1.4 ($HFSG_2$) and −3.6 ($HFSG_3$) mV, respectively. The decrease in the net ζ-potential indicates a heightened collision frequency among particles, the presence of unfolded proteins within the particles, and the exposure of hydrophobic patches. This sequence of factors initiates the aggregation of particles, leading to a reduction in the overall stability of the system (Joye, Davidov-Pardo, Ludescher, & McClements, 2015). Moreover, the net ζ-potential of FSG decreased from −24.8 to −18.6 mV after loading curcumin. This might be ascribed to the decrease in negative charge density for FSG caused by the curled, tangled threads of protein on the

inside of the gelatin structure (Dai, Reichert, Hinrichs, & Weiss, 2019). To the contrary, the net ζ-potential of HFSG simultaneously and interestingly increased after loading curcumin. This result indicated that HFSG might be electrostatically attracted by the curcumin, resulting in an augmented negative charge density of the outer hydrophilic shell. It could be thus concluded that this higher surface charge contributes to a lower aggregation tendency of protein particles because the hydrophilic groups in the protein solution provide sufficient electrostatic repulsion away from adjacent protein particles.

3.5. Possible curcumin loading mechanism of acid-induced hydrolysis of FSG

CLSM was used to further characterize the morphology of CL-FSG and CL-HFSG$_{1\text{-}3}$ nanoparticles and the interaction between curcumin and FSG with or without acid hydrolysis. As shown in Fig. 7(A), the green-colored particle sizes of FSG (curcumin-1) were larger than those observed for HFSG (curcumin-2, curcumin-3, and curcumin-4). The particle sizes of the red-colored particles (soluble gelatin molecule) consistently exhibited a comparable trend to that observed for the green particles. This could be attributed to acid hydrolysis; the larger aggregates of FSG were decomposed into smaller particles with lower M_w, providing favorable conditions for dispersal in solvent. Compared with

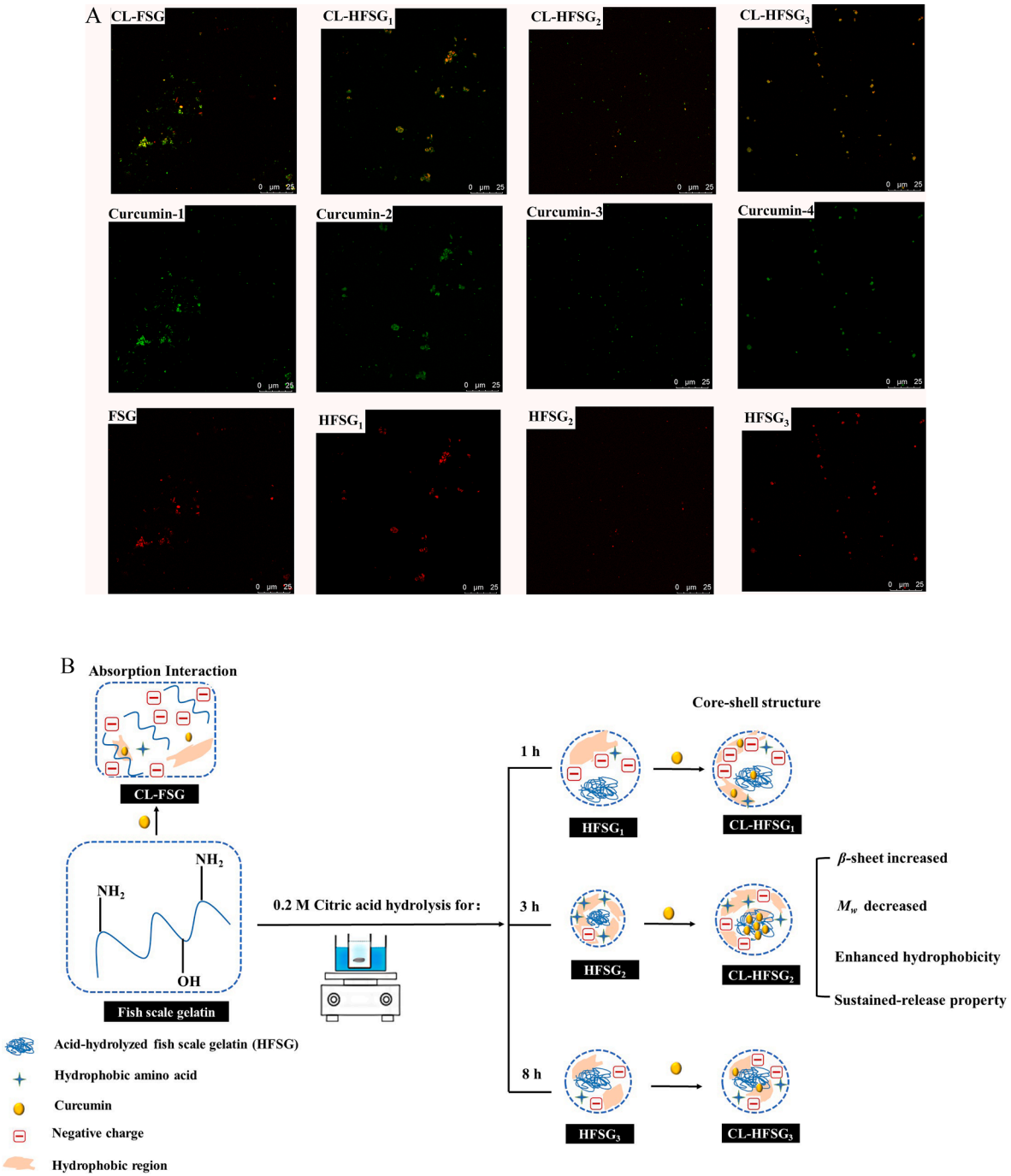

Fig. 7. CLSM images (A) and schematic diagram (B) of curcumin loading mechanism of FSG (fish scale gelatin) and HFSGs (HFSG$_1$, duration of acid hydrolysis = 1 h; HFSG$_2$, duration of acid hydrolysis = 3 h; HFSG$_3$, duration of acid hydrolysis = 8 h).

partially overlapping distribution as observed in the FSG-curcumin matrix, the $HFSG_1$ and $HFSG_3$ nanoparticles (stained with rhodamine B) exhibited a homogenous distribution and displayed a nearly perfect colocalization with curcumin nanoparticles. This suggests that $HFSG_1$ and $HFSG_3$ nanoparticles shared the same mechanism for loading curcumin. Specifically, the curcumin nanoparticles were uniformly incorporated into the matrix of $HFSG_1$ and $HFSG_3$ nanoparticles through hydrophobic interactions between curcumin and these nanoparticles. Nevertheless, CL-$HFSG_2$ indicated a distinct curcumin loading mechanism of two types: 1) resembling CL-$HFSG_1$ or CL-$HFSG_3$, where the red- and green-colored spots in the CLSM of CL-$HFSG_2$ were colocalized; 2) featuring only isolated red- or green-colored spots scattered in the CLSM.

As illustrated in Fig. 7(B), the unique loading mechanism of HFSG imbues it with an advantageous capacity for loading curcumin. The changes in curcumin loading capacity (CLC) observed during the continuous acid hydrolysis of HFSG could be ascribed to two factors: 1) the acidic treatment of FSG induces the degradation of gelatin, as evidenced by the decreased M_w. This decrease makes the hydrophobic regions of FSG more susceptible to disruption during the degradation of the molecular skeleton. The hydrophobic cavity within HFSG underwent enhanced solidification by the aid of hydrophobic interactions and disulfide bonds among $HFSG_{1\text{-}2}$ groups, as mentioned above in the intermolecular interaction's measurement. This emphasizes the contribution of moderate acid hydrolysis to facilitating the formation and expansion of hydrophobic cores within the core–shell structure through self-assembly. As a result, this configuration becomes more favorable for the encapsulation of curcumin in the core–shell structure; 2) $HFSG_{1\text{-}3}$ exhibit a relatively higher surface hydrophobicity compared to FSG, promoting the unfolding of gelatin, and exposing its embedded hydrophobic groups. Furthermore, compared with the solubility of curcumin powder in water of 11 ng/mL (Aliabadi, Mahmud, Sharifabadi, & Lavasanifar, 2005), the solubility of $HFSG_2$ is increased by orders of magnitude to approximately 1663 times. This suggests that during the initial stage of acid hydrolysis, the interior hydrophobic groups within HFSG were prone to exposure, accompanied by a decrease in M_w. This heightened exposure raised the possibility for interactions between curcumin molecules and hydrophobic groups of HFSG.

3.6. *In vitro simulated gastrointestinal behavior of curcumin-loaded FSG (CL-FSG) and acid-hydrolyzed FSG (CL-HFSG)*

Curcumin molecules are prone to chemical degradation in aqueous environments, with reported degradation reaching as high as 90 % after 30 min of aqueous storage at room temperature at neutral pH (Naksuriya et al., 2016). To investigate the potential protective effect of nanocarriers constructed by the acid hydrolysis of FSG, the degradation and release rates for free curcumin, CL-FSG, and CL-$HFSG_2$ were assessed through *in vitro* simulation of digestion. As depicted in Fig. 8(A), after the completion of simulated gastric fluid digestion, the retention rate of free curcumin in the solution decreased by 53.7 %. Conversely, curcumin within the CL-FSG and CL-HFSG nanoparticles showed a noteworthy retention rate diminished by only 10 %. Following a six-hour digestion in simulated intestinal fluid, there was a substantial reduction in the retention rate for free curcumin (81.2 %). In comparison, the retention rates for CL-FSG and CL-$HFSG_2$ underwent decreases of 58.2 % and 23.9 %, respectively (Fig. 8B). Free curcumin exhibited notable instability, i.e., a low retention rate in aqueous solutions, with the result being pronounced degradation. In contrast, the curcumin stability of CL-$HFSG_2$ nanoparticles was remarkably superior to that of CL-FSG

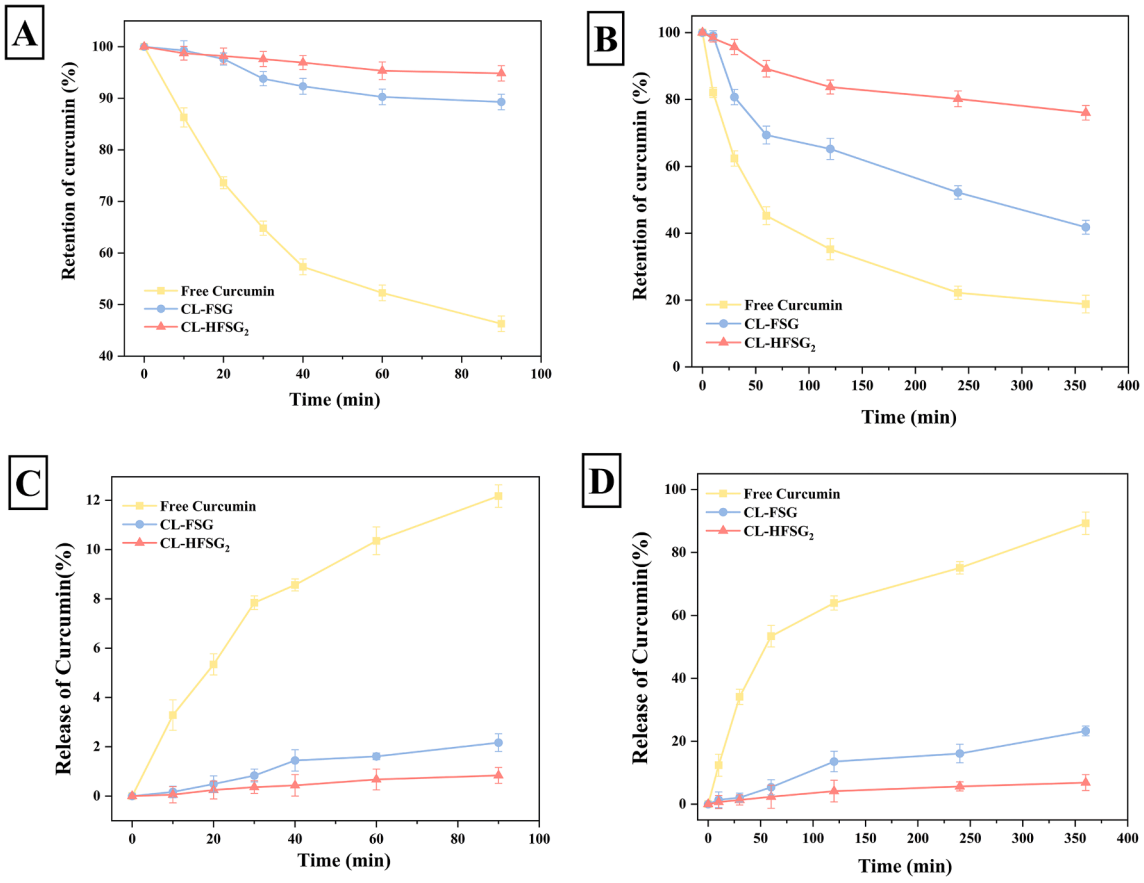

Fig. 8. In vitro simulated gastric (A and C) and intestinal (B and D) stability and release of free curcumin, curcumin loaded fish scale gelatin (CL-FSG) and curcumin loaded fish scale gelatin subjected to acid hydrolysis for 3 h (CL-$HFSG_2$).

nanoparticles. This phenomenon can be attributed to subjecting FSG to appropriate acid hydrolysis, thereby promoting the formation of more intensified hydrophobic interactions. These interactions effectively preserved the stability of the hydrophobic cavity structure in HFSG, implying that the observed disparity in curcumin stability is closely linked to its specific location within the nanoparticle (Ji et al., 2023). Furthermore, as shown in Fig. 8 (C - D), in contrast to free curcumin (with a curcumin release rate at the end of digestion of 12.2 % in the gastric region and 89.3 % in the intestinal region), both CL-FSG and CL-$HFSG_2$ demonstrated greater efficiency in impeding the release of curcumin in simulated gastric and intestinal fluids. Following simulated digestion, the curcumin release rates were confined to the narrow ranges of 0.8 % to 2.1 % (in the gastral region) and 6.9 % to 23.3 % (in the intestine region). Additionally, the self-assembly of $HFSG_2$ through acid hydrolysis further lowered the release rate of curcumin, achieving a beneficial sustained-release effect. This phenomenon might be ascribed to the acid-induced exposure of the hydrophobic region in $HFSG_2$, effectively restricting the diffusion of encapsulated curcumin molecules. Furthermore, previous fluorescence spectra and XPS results indicated that $HFSG_2$ exhibited strengthened binding affinity to curcumin, offering additional prospects for the controlled release of bioactive substances into the intestine.

The bioaccessibility and bioavailability of curcumin in free curcumin, CL-FSG, and CL-$HFSG_2$ are illustrated in Fig. S3. The bioaccessibility of curcumin relies on its solubility in digestive fluid, a heightened solubility corresponding directly to an increased level of bioaccessibility (Teng et al., 2012). Free curcumin displayed a minimal transfer of only 28.3 % to the aqueous phase throughout the process. However, 68.2 % and 87.5 % of curcumin loaded in CL-FSG and CL-$HFSG_2$ nanoparticles were transferred into the aqueous phase after the intestinal digestion phase. This can be attributed to the enhanced hydrophobicity of FSG resulting from acid hydrolysis, effectively increasing the solubility of curcumin. On the other hand, CL-$HFSG_2$ exhibited an impressive bioavailability of 52.2 %, exceeding that of free curcumin (4.3 %) by a factor of 12.16, implying the establishment of a stable microenvironment by CL-$HFSG_2$, facilitating the sustained release of curcumin during the digestive process.

4. Conclusion

This study delved into the impact of acid hydrolysis on both the structural and functional aspects of FSG, shedding light on its interactions with curcumin. Notably, the duration of acid hydrolysis emerged as a critical factor influencing the curcumin loading capacity (CLC) of FSG. During the initial three hours of moderate acid hydrolysis, structural modifications to HFSG resulted in a decreased M_w and exposed hydrophobic groups and heightened hydrophobicity, thereby leading to a substantial increase in CLC. These modifications coincided with a more flexible, linear structure and an augmented proportion of β-sheet structure. However, as acid hydrolysis was extended beyond the initial stage, no additional improvement in CLC was observed. Moreover, appropriate acid hydrolysis enhanced hydrophobic interactions between HFSG and curcumin, whereas excessive acid hydrolysis of FSG exerted an adverse effect with weaker hydrophobic interactions, which was attributed to the further decrease in M_w, that resulted in the disruption of the intramolecular hydrophobic regions. As a result, compared to curcumin-loaded FSG, the curcumin-loaded HFSG demonstrated exceptional bioaccessibility and bioavailability coupled with remarkable sustained-release properties during the simulated gastrointestinal digestion process. In general, this work provides a facile and cost-saving method for the construction of protein-based nanoparticles as a promising delivery system for hydrophobic bioactive substances.

CRediT authorship contribution statement

Haoxin Li: Conceptualization, Resources, Software, Validation, Writing – original draft. **Wan Aida Wan Mustapha:** Investigation, Methodology. **Jia Liu:** Data curation, Formal analysis, Investigation, Methodology, Writing – review & editing. **Xiaoping Zhang:** Data curation, Formal analysis.

Declaration of competing interest

The authors declare that they have no known competing financial interests or personal relationships that could have appeared to influence the work reported in this paper.

Data availability

Data will be made available on request.

Acknowledgments

This work was supported by the Guizhou Provincial Science and Technology Foundation (ZK [2023]-334), National Natural Science Foundation of China, Grant/Award Number (32060545 and 32260602). We thank consultant Mark Inglin for scientific and editorial assistance. In addition, the authors would like to thank Shiyanjia Lab (www.shiyanjia.com) for facilitating CLSM and TEM analysis.

Appendix A. Supplementary data

Supplementary data to this article can be found online at https://doi.org/10.1016/j.fochx.2024.101230.

References

Acevedo, C. A., Sánchez, E., Díaz-Calderón, P., Blaker, J. J., Enrione, J., & Quero, F. (2017). Synergistic effects of crosslinking and chitosan molecular weight on the microstructure, molecular mobility, thermal and sorption properties of porous chitosan/gelatin/hyaluronic acid scaffolds. *Journal of Applied Polymer Science, 134* (18).

Aidat, O., Belkacemi, L., Belalia, M., Zainol, M. k., & Barhoum, H. S. (2023). Physicochemical, rheological, and textural properties of gelatin extracted from chicken by-products (feet-heads) blend and application. *International Journal of Gastronomy and Food Science, 32*, 100708.

Aliabadi, H. M., Mahmud, A., Sharifabadi, A. D., & Lavasanifar, A. (2005). Micelles of methoxy poly (ethylene oxide)-b-poly(ε-caprolactone) as vehicles for the solubilization and controlled delivery of cyclosporine A. *Journal of Controlled Release, 104*(2), 301-311.Bertsch, M., Mayburd, A. L., & Kassner, R. J. (2003). The identification of hydrophobic sites on the surface of proteins using absorption difference spectroscopy of bromophenol blue. *Analytical Biochemistry, 313*(2), 187-195.

Bhat, R., & Karim, A. A. (2009). Ultraviolet irradiation improves gel strength of fish gelatin. *Food Chemistry, 113*(4), 1160–1164.

Cen, S., Zhang, L., Liu, L., Lou, Q., Wang, C., & Huang, T. (2022). Phosphorylation modification on functional and structural properties of fish gelatin: The effects of phosphate contents. *Food Chemistry, 380*, Article 132209.

Chen, Y., Wang, Y., Liu, R., Xiong, S., Xu, Y., & Hu, Y. (2023). Effects of microbial transglutaminase on the gelling property and in vitro digestibility of fish scale gelatin from grass carp. *Food Bioscience, 53*, Article 102569.

Chua, L.-K., Lim, P.-K., Thoo, Y.-Y., Neo, Y.-P., & Tan, T.-C. (2023). Extraction and characterization of gelatin derived from acetic acid-treated black soldier fly larvae. *Food Chemistry Advances, 2*, Article 100282.

Dai, L., Reichert, C. L., Hinrichs, J., & Weiss, J. (2019). Acid hydrolysis behavior of insoluble protein-rich fraction extracted from Chlorella prototheocoides. *Colloids and Surfaces A: Physicochemical and Engineering Aspects, 569*, 129–136.

Du, J., Hong, Y., Cheng, L., Gu, Z., Li, Z., & Li, C. (2022). Effects of acid-ethanol hydrolysis and debranch on acetylated starch and its potential used for curcumin carrier. *Carbohydrate Polymers, 279*, Article 119019.

Gopal, R., Park, J. S., Seo, C. H., & Park, Y. (2012). Applications of circular dichroism for structural analysis of gelatin and antimicrobial peptides. *International Journal of Molecular Sciences, 13*(3), 3229–3244.

Hao, X., Shen, W., Chen, Z., Zhu, J., Feng, L., Wu, Z., & Wu, T. (2015). Self-assembled nanostructured cellulose prepared by a dissolution and regeneration process using phosphoric acid as a solvent. *Carbohydrate Polymers, 123*, 297–304.

He, L., Gao, Y., Wang, X., Han, L., Yu, Q., Shi, H., & Song, R. (2021). Ultrasonication promotes extraction of antioxidant peptides from oxhide gelatin by modifying collagen molecule structure. *Ultrasonics Sonochemistry, 78*, Article 105738.

Huang, T., Tu, Z. c., Shangguan, X., Sha, X., Wang, H., Zhang, L., & Bansal, N. (2019). Fish gelatin modifications: A comprehensive review. *Trends in Food Science & Technology, 86*, 260-269.

Huang, T., Tu, Z. c., Shangguan, X., Wang, H., Sha, X., & Bansal, N. (2018). Rheological behavior, emulsifying properties and structural characterization of phosphorylated fish gelatin. *Food Chemistry, 246*, 428-436.

Huang, T., Tu, Z. c., Wang, H., Shangguan, X., Zhang, L., Zhang, N.-h., & Bansal, N. (2017). Pectin and enzyme complex modified fish scales gelatin: Rheological behavior, gel properties and nanostructure. *Carbohydrate Polymers, 156*, 294-302.

Huang, X., Liu, Y., Zou, Y., Liang, X., Peng, Y., McClements, D. J., & Hu, K. (2019). Encapsulation of resveratrol in zein/pectin core-shell nanoparticles: Stability, bioaccessibility, and antioxidant capacity after simulated gastrointestinal digestion. *Food Hydrocolloids, 93*, 261–269.

Jafari, S. M., Assadpoor, E., Bhandari, B., & He, Y. (2008). Nano-particle encapsulation of fish oil by spray drying. *Food Research International, 41*(2), 172–183.

Ji, F., Xu, J., Liu, H., Shao, D., Wang, C., Zhao, Y., Luo, S., Zhong, X., & Zheng, Z. (2023). Improved water solubility, antioxidant, and sustained-release properties of curcumin through the complexation with soy protein fibrils. *LWT-Food Science and Technology, 180*, Article 114723.

Jiang, J., Chen, J., & Xiong, Y. L. (2009). Structural and emulsifying properties of soy protein isolate subjected to acid and alkaline pH-shifting processes. *Journal of Agricultural and Food Chemistry, 57*(16), 7576–7583.

Jongjareonrak, A., Benjakul, S., Visessanguan, W., & Tanaka, M. (2006). Skin gelatin from bigeye snapper and brownstripe red snapper: Chemical compositions and effect of microbial transglutaminase on gel properties. *Food Hydrocolloids, 20*(8), 1216–1222.

Joye, I. J., Davidov-Pardo, G., Ludescher, R. D., & McClements, D. J. (2015). Fluorescence quenching study of resveratrol binding to zein and gliadin: Towards a more rational approach to resveratrol encapsulation using water-insoluble proteins. *Food Chemistry, 185*, 261–267.

Kaewruang, P., Benjakul, S., & Prodpran, T. (2014). Effect of phosphorylation on gel properties of gelatin from the skin of unicorn leatherjacket. *Food Hydrocolloids, 35*, 694–699.

Karim, A. A., & Bhat, R. (2009). Fish gelatin: Properties, challenges, and prospects as an alternative to mammalian gelatins. *Food Hydrocolloids, 23*(3), 563–576.

Kołodziejska, I., Skierka, E., Sadowska, M., Kołodziejski, W., & Niecikowska, C. (2008). Effect of extracting time and temperature on yield of gelatin from different fish offal. *Food Chemistry, 107*(2), 700–706.

Lamp, A., Kaltschmitt, M., & Lüdtke, O. (2018). Improved HPLC-method for estimation and correction of amino acid losses during hydrolysis of unknown samples. *Analytical Biochemistry, 543*, 140–145.

Lazaridou, A., Biliaderis, C. G., & Izydorczyk, M. S. (2003). Molecular size effects on rheological properties of oat β-glucans in solution and gels. *Food Hydrocolloids, 17*(5), 693–712.

Li, H., Wan Mustapha, W. A., Tian, G., Dong, N., Zhao, F., Zhang, X., Long, D., & Liu, J. (2024). Enhanced hydrophobic interaction between fish (Cyprinus carpio L.) scale gelatin and curcumin: Mechanism study. *Food Chemistry, 431*, Article 137102.

Li, J., Tang, W., Lei, Z., Wang, Z., & Liu, J. (2021). Effect of polysaccharides on the gel characteristics of "Yu Dong" formed with fish (Cyprinus carpio L.) scale aqueous extract. *Food Chemistry, 338*, Article 127792.

Li, J., Yu, X., Tang, W., Wan, C., Lu, Y., Dong, N., & Liu, J. (2021). Characterization of food gels prepared from the water extract of fish (Cyprinus carpio L.) scales: From molecular components to sensory attributes. *Food Hydrocolloids, 112*, Article 106263.

Li, T., Wang, C., Li, T., Ma, L., Sun, D., Hou, J., & Jiang, Z. (2018). Surface Hydrophobicity and Functional Properties of Citric Acid Cross-Linked Whey Protein Isolate: The Impact of pH and Concentration of Citric Acid. *Molecules, 23*(9), 2383.

Li, Z., Lin, Q., McClements, D. J., Fu, Y., Xie, H., Li, T., & Chen, G. (2021). Curcumin-loaded core-shell biopolymer nanoparticles produced by the pH-driven method: Physicochemical and release properties. *Food Chemistry, 355*, Article 129686.

Liang, S., Du, J., Hong, Y., Cheng, L., Gu, Z., Li, Z., & Li, C. (2023). Octenyl succinate anhydride debranched starch-based nanocarriers for curcumin with improved stability and antioxidant activity. *Food Hydrocolloids, 135*, Article 108118.

Linden, E., & Venema, P. (2007). Self-assembly and aggregation of proteins. *Current Opinion in Colloid & Interface Science, 12*, 158–165.

Liu, J., Li, J., Ma, Y., Chen, F., & Zhao, G. (2013). Synthesis, Characterization, and Aqueous Self-Assembly of Octenylsuccinate Oat β-Glucan. *Journal of Agricultural and Food Chemistry, 61*(51), 12683–12691.

Liu, Y., Chen, X., Yin, S., Chang, X., Lv, C., Zang, J., & Zhao, G. (2022). Directed Self-Assembly of Dimeric Building Blocks into Networklike Protein Origami to Construct Hydrogels. *ACS Nano, 16*(11), 19472–19481.

Mohtar, N. F., Perera, C. O., & Hemar, Y. (2014). Chemical modification of New Zealand hoki (Macruronus novaezelandiae) skin gelatin and its properties. *Food Chemistry, 155*, 64–73.

Naksuriya, O., van Steenbergen, M. J., Torano, J. S., Okonogi, S., & Hennink, W. E. (2016). A Kinetic Degradation Study of Curcumin in Its Free Form and Loaded in Polymeric Micelles. *AAPS Journal, 18*(3), 777–787.

Nitsuwat, S., Zhang, P., Ng, K., & Fang, Z. (2021). Fish gelatin as an alternative to mammalian gelatin for food industry: A meta-analysis. *LWT-Food Science and Technology, 141*, Article 110899.

Nourbakhsh, H., Emam-Djomeh, Z., Madadlou, A., Mousavi, M. E., Moosavi-Movahedi, A. A., & Gunasekaran, S. (2017). Antioxidant Peptidic Particles for Delivery of Gallic Acid. *Journal of Food Processing and Preservation, 41*(1), 12767.

Pan, K., Luo, Y., Gan, Y., Baek, S. J., & Zhong, Q. (2014). pH-driven encapsulation of curcumin in self-assembled casein nanoparticles for enhanced dispersibility and bioactivity. *Soft Matter, 10*(35), 6820–6830.

Pan, K., & Zhong, Q. (2016). Low energy, organic solvent-free co-assembly of zein and caseinate to prepare stable dispersions. *Food Hydrocolloids, 52*, 600–606.

Saxena, A., Sachin, K., Bohidar, H. B., & Verma, A. K. (2005). Effect of molecular weight heterogeneity on drug encapsulation efficiency of gelatin nanoparticles. *Colloids and Surfaces B: Biointerfaces, 45*(1), 42–48.

Sha, X.-M., Tu, Z.-C., Liu, W., Wang, H., Shi, Y., Huang, T., & Man, Z.-Z. (2014). Effect of ammonium sulfate fractional precipitation on gel strength and characteristics of gelatin from bighead carp (Hypophthalmichthys nobilis) scale. *Food Hydrocolloids, 36*, 173–180.

Shi, K., Kokini, J. L., & Huang, Q. (2009). Engineering zein films with controlled surface morphology and hydrophilicity. *Journal of Agricultural and Food Chemistry, 57*(6), 2186–2192.

Sow, L. C., & Yang, H. (2015). Effects of salt and sugar addition on the physicochemical properties and nanostructure of fish gelatin. *Food Hydrocolloids, 45*, 72–82.

Teng, Z., Luo, Y., & Wang, Q. (2012). Nanoparticles Synthesized from Soy Protein: Preparation, Characterization, and Application for Nutraceutical Encapsulation. *Journal of Agricultural and Food Chemistry, 60*(10), 2712–2720.

Uriarte-Montoya, M. H., Santacruz-Ortega, H., Cinco-Moroyoqui, F. J., Rouzaud-Sández, O., Plascencia-Jatomea, M., & Ezquerra-Brauer, J. M. (2011). Giant squid skin gelatin: Chemical composition and biophysical characterization. *Food Research International, 44*(10), 3243–3249.

Wang, H., Williams, P. A., & Senan, C. (2014). Synthesis, characterization and emulsification properties of dodecenyl succinic anhydride derivatives of gum Arabic. *Food Hydrocolloids, 37*, 143–148.

Wang, L., Xue, J., & Zhang, Y. (2019). Preparation and characterization of curcumin loaded caseinate/zein nanocomposite film using pH-driven method. *Industrial Crops and Products, 130*, 71–80.

Wu, W., Xu, J., Yang, L., Yang, M., Zhang, T., Wang, X., & Zhong, J. (2022). Self-assembled hydrolyzed gelatin nanoparticles from silver carp spine bones for Pickering emulsion stabilization. *Food Bioscience, 48*, Article 101735.

Yang, X., Su, Y., & Li, L. (2020). Study of soybean gel induced by Lactobacillus plantarum: Protein structure and intermolecular interaction. *LWT - food science and technology, 119*, Article 108794.

Yu, X., Li, H., Wan, A. W., Ren, T., Lei, Z., & Liu, J. (2022). Curcumin-Loaded Self-Assembly Constructed by Octenylsuccinate Fish (Cyprinus carpio L.) Scale Gelatin. *Preparation and Characterization. Foods, 11*, 2911.

Zhang, T., Sun, R., Ding, M., Tao, L., Liu, L., Tao, N., & Zhong, J. (2020). Effect of extraction methods on the structural characteristics, functional properties, and emulsion stabilization ability of Tilapia skin gelatins. *Food Chemistry, 328*, Article 127114.